Original contribution

Multi-modal imaging with specialized sequences improves accuracy of the automated subcortical grey matter segmentation

Andrew J. Plassard[a], Shunxing Bao[a,*], Pierre F. D'Haese[b], Srivatsan Pallavaram[b], Daniel O. Claassen[c], Benoit M. Dawant[a,b], Bennett A. Landman[a,b]

[a] Computer Science, Vanderbilt University, 2301 Vanderbilt Place, Nashville, TN 37235, USA
[b] Electrical Engineering, Vanderbilt University, 2301 Vanderbilt Place, Nashville, TN 37235, USA
[c] Neurology, Vanderbilt University, 2301 Vanderbilt Place, Nashville, TN 37235, USA

ABSTRACT

The basal ganglia and limbic system, particularly the thalamus, putamen, internal and external globus pallidus, substantia nigra, and sub-thalamic nucleus, comprise a clinically relevant signal network for Parkinson's disease. In order to manually trace these structures, a combination of high-resolution and specialized sequences at 7 T are used, but it is not feasible to routinely scan clinical patients in those scanners. Targeted imaging sequences at 3 T have been presented to enhance contrast in a select group of these structures. In this work, we show that a series of atlases generated at 7 T can be used to accurately segment these structures at 3 T using a combination of standard and optimized imaging sequences, though no one approach provided the best result across all structures. In the thalamus and putamen, a median Dice Similarity Coefficient (DSC) over 0.88 and a mean surface distance < 1.0 mm were achieved using a combination of T1 and an optimized inversion recovery imaging sequences. In the internal and external globus pallidus a DSC over 0.75 and a mean surface distance < 1.2 mm were achieved using a combination of T1 and inversion recovery imaging sequences. In the substantia nigra and sub-thalamic nucleus a DSC of over 0.6 and a mean surface distance of < 1.0 mm were achieved using the inversion recovery imaging sequence. On average, using T1 and optimized inversion recovery together significantly improved segmentation results than over individual modality ($p < 0.05$ Wilcoxon sign-rank test).

1. Introduction

The subcortical grey matter is a collection of nuclei situated near the forebrain [1]. These nuclei are primarily involved in connecting distinct portions of the brain, to serve as major functional systems within the brain [1]. For instance, the globus pallidus internal receives GABAergic signaling from the putamen and relays that to the sub-thalamic nucleus. Many subcortical structures have been implicated in one or more diseases [2]. In addition, dopamine is dysregulated in the putamen and adjacent structures causing dependence phenotypes [3]. In Parkinson's disease, several subcortical structures undergo Lewy body growth and that growth plays a significant role in the motor phenotypes associated with the disease [4].

Recently, specialized imaging sequences have been developed for studying subcortical grey matter using clinical magnetic resonance (MR) scanners. In particular, the Fast Grey Matter Acquisition T1 Inversion Recovery (FGATIR) sequence was developed to improve subcortical grey matter contrast with the surrounding tissue [5]. The

FGATIR sequence uses a longer inversion time than standard T1-weighted approaches, such as Magnetization Prepared Rapid Acquisition Gradient Echo (MPRAGE), to null the white matter and accentuate the deep brain structures. FGATIR images accentuate the sub-thalamic nucleus, lamina separating the internal and external globus pallidus, and the thalamus amongst other important structures. On the other hand, many important subcortical structures are still difficult to parcellate using the FGATIR [6]. Higher field strength scanners are needed, but these scans at higher field strengths are not clinically feasible in most contexts [7].

In this work, we investigate the efficacy of sequences acquirable in a clinically tolerable setting, namely standard T1-weighted MPRAGE scans and T1-weighted FGATIR scans acquired at 3 T. The structures considered in this work are the substantia nigra (SN), subthalamic nucleus (STN), internal globus pallidus (GPI), external globus pallidus (GPE), putamen, and thalamus. These subcortical structures were manually delineated using a combination of scans acquired at 3 T and 7 T. Furthermore, we compare segmentation using only one modality,

either the MPRAGE or FGATIR, to multi-modal segmentation using the enhanced and complimentary contrast patterns present to improve the overall segmentation results. The primary aspect of novelty of this work is the investigation of multi-modal MRI in the context of subcortical segmentation.

2. Methods

We propose a multi-atlas segmentation algorithm for automated segmentation of the subcortical grey matter. This approach uses multi-modal atlases derived using imaging acquired at 3 T and 7 T. The segmentation uses the imaging sequences acquired at 3 T to assess the effectiveness of segmenting subcortical structures using clinically feasible acquisitions.

2.1. Atlas imaging

Nine healthy subjects were scanned at 3 T and 7 T. At 7 T, a series of 0.7 mm isotropic T1-weighted MPRAGE (Inversion Time (TI)/ Repetition Time (TR)/Echo Time (TE) = [400,640,960,1120]/4.74/ 2.09 ms) was acquired and a susceptibility weighted image slab through the midbrain acquired at $0.2 \times 0.2 \times 1.1$ mm was acquired sagitally, coronally, and axially (TR/TE/Flip Angle (FA) = 1952/23 ms/45° for all orientations). At 3 T, a 1.0 mm isotropic resolution T1-weighted MP-RAGE (TI/TR/TE = 925/8.1/2.7 ms) and an FGATIR scan was acquired for additional mid-brain contrast (TI/TR/TE = 400/7.39/3.43).

2.2. Manual segmentation

For each subject, the 7 T T1-weighted MP-RAGE with the inversion time of 960 ms was used as the reference space. The other 7 T MP-RAGE scans, 3 T MP-RAGE, 7 T high-resolution susceptibility weighted slabs, and 3 T FGATIR were co-registered to the reference space. The following structures were manually labeled on the left hemisphere for one subject: GPI, GPE, STN, SN, thalamus, and the putamen. The labeled atlas was then registered to each of the other eight subjects and the labels were deformed to the target space using the Reg Aladin rigid affine transformation algorithm in NiftyReg [8]. The deformed labels were then manually corrected. Finally, each subject was flipped laterally and the flipped image was registered to the standard space image. Each subject's labels were deformed in the laterally flipped space and the results were manually corrected. The final result was nine subjects with left and right labels for the GPI, GPE, STN, SN, thalamus, and putamen. All manual segmentations were done using CranialVault and the CRAVE Tools [9] (by Pierre F. D'Haese).

2.3. Segmentation algorithm

First, each subject, the 3 T T1-weighted MRI was automatically segmented with the BrainCOLOR protocol [10] (www. neuromorphometrics.com) following a standard multi-atlas whole brain segmentation (WBS) approach [11]. Briefly, the target image was affinely registered to MNI space. From a population of 45 atlases (45 T1w MRI scans from Open Access Series on Imaging Studies (OASIS) dataset [12] with BrainCOLOR labeling protocol are considered as the 45 atlases), the 15 atlases geodesically most similar to the target are then empirically selected [13]. These 15 atlases are non-rigidly registered to the target image using the Advance Normalization Tools (ANTs) Symmetric Normalization algorithm (SyN) [14]. Finally, the registered atlas images and labels are fused to the target image using Hierarchical Non-Local Spatial STAPLE [15].

Thus, WBS was used to localize the particular regions of interest. In particular, the thalamus label from the WBS was used to localize the thalamus, the globus pallidus and putamen labels from the WBS were used to localize the GPI, GPE, and putamen, and the diencephalon label from the WBS was used to localize the SN and STN. The bounding box

of each of these regions of interest was identified and dilated by 5 mm. Finally, the labels and T1 and FGATIR intensities were extracted from these bounding boxes and saved as reduced field of view (RFOV) atlases.

For a given target, the target was segmented with the BrainCOLOR protocol. A series of targets (RFOV) were created following the protocol defined above. The RFOV atlases were co-registered to the RFOV targets. All registrations were performed using with ANTs and the SyN algorithm [16]. After registration, joint label fusion (JLF) was used. In all cases, the same collection of imaging modalities was used for the segmentation [17]. Finally, each structure's segmentation was re-inserted into the standard image space. All operations for creating and manipulating using RFOV atlases and images used custom MATLAB (www.mathworks.org) code.

3. Results

Each of the nine healthy subjects was segmented in a leave-one-out cross validation scheme. First, each subject was segmented using the T1-weighted MRI, the FGATIR, and multi-modally with the T1 and FGATIR. Second, each subject's scans were flipped left-right to produce a second set of atlases. Each subject was then segmented with the 16 atlases, leaving out the atlas and the flipped version of the atlas. As a result, each subject was segmented six times, twice with each combination of modalities. The results are divided into three pieces for ease of visualization: diencephalon (STN and SN), GPI and GPE, and thalamus and putamen. For each segmentation result the Dice Similarity Coefficient (DSC), mean surface distance (MSD), and Hausdorff distance (HD) were calculated.

3.1. Diencephalon

Four structures were segmented in the diencephalon: the left STN, right STN, left SN, and right SN (Fig. 1). For the left SN, the segmentation with T1 and FGATIR outperformed other approaches (p < 0.05 Wilcoxon sign-rank test) with a median DSC of 0.65, median MSD of 0.98 mm, and a median HD of 3.11 mm. For the right SN, no approach significantly outperformed other approaches. For the left STN, segmentation with T1 and FGATIR outperformed other approaches (p < 0.05 Wilcoxon sign-rank test) with a median DSC of 0.70, median MSD of 0.61 mm, and a median HD of 2.06 mm. For the right STN, no approach outperformed other approaches (Wilcoxon sign-rank test).

3.2. Globus pallidus

Two structures were segmented in the globus pallidus: the GPI and GPE. These structures were segmented bilaterally and resulted in four total structures segmented (Fig. 2). For the left GPE, the segmentation with T1 and FGATIR including flipped atlases outperformed other approaches (p < 0.05 Wilcoxon sign-rank test) with a median DSC of 0.68, median MSD of 0.94 mm, and a median HD of 2.70 mm. For the right GPE, segmentation with FGATIR outperformed other approaches (p < 0.05 Wilcoxon sign-rank test) with a median DSC of 0.71, a median MSD of 0.96 mm, and a median HD of 3.42 mm. For the left GPI, segmentation with FGATIR with flipped atlases and multi-modal segmentation with T1 and FGATIR and flipped atlases outperformed other approaches but were not statistically distinguishable from each other (p < 0.05 Wilcoxon sign-rank test), with median DSC values of 0.80 and 0.81, median MSD values of 0.68 and 0.69 mm, and median HD values of 2.50 and 2.52 mm respectively. For the right GPI, no approach significantly outperformed another.

3.3. Thalamus and putamen

The left and right thalamus and putamen were segmented resulting in four total structures (Fig. 3). For the left putamen the segmentation
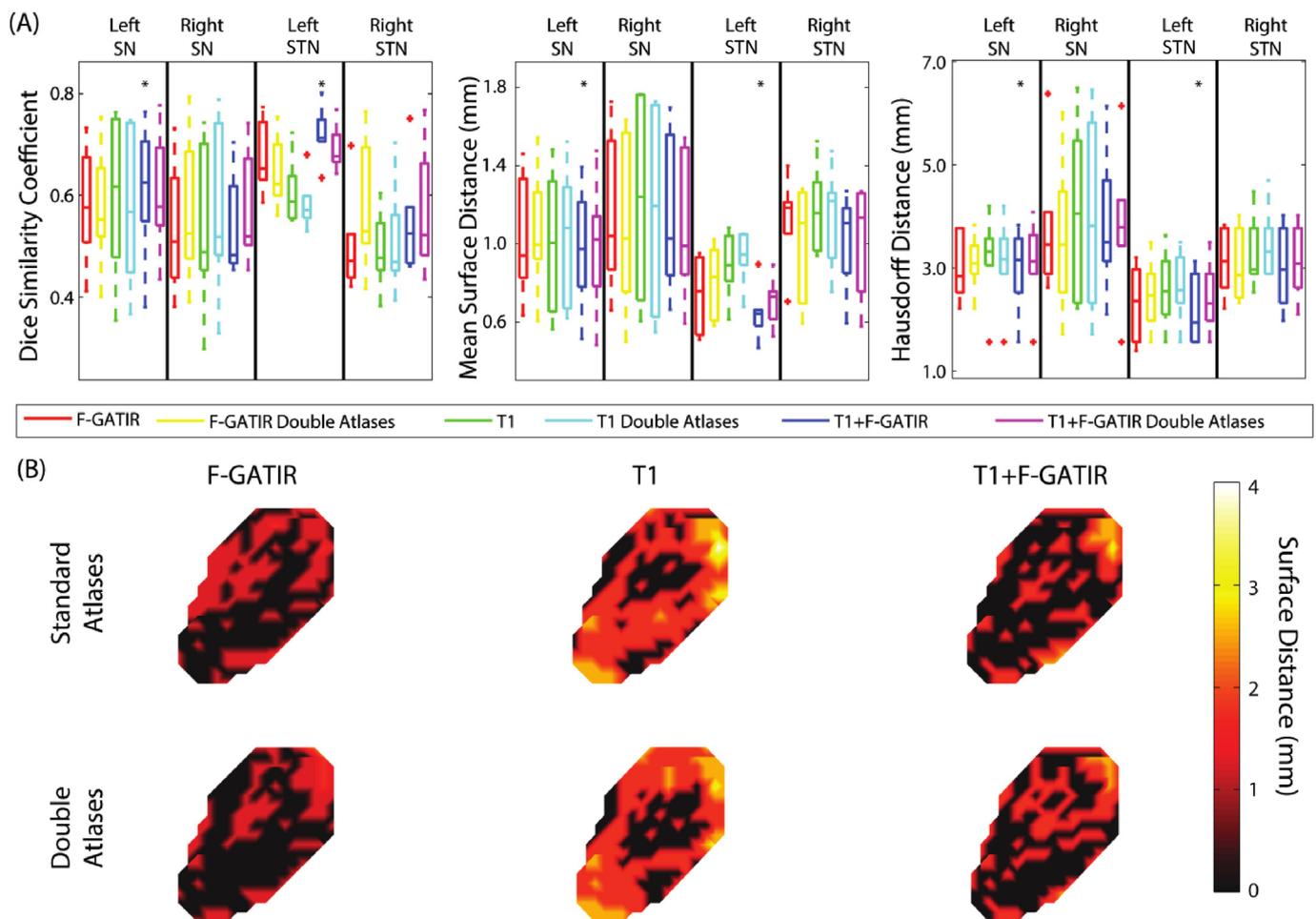
Fig. 1. Segmentation results for structures in the dienchephalon. Quantitative segmentation results are shown in (A). For the left SN, multi-modal segmentation with T1 and FGATIR outperformed other approaches (*; p < 0.05; Wilcoxon sign-rank test). For the right SN no segmentation approach outperformed other approaches. For the left STN, multi-modal segmentation with T1 and FGATIR outperformed other approaches (*; p < 0.05; Wilcoxon sign-rank test). For the right STN no segmentation approach outperformed other approaches. In (B), surface distances between the true and estimated segmentations for the left SN are shown for the six proposed segmentation approaches.

with T1 and FGATIR including flipped atlases outperformed other approaches (p < 0.05 Wilcoxon sign-rank test) with a median DSC of 0.93, a median MSD of 0.42 mm, and a median HD of 2.50 mm. For the right putamen, segmentation with FGATIR including flipped atlases outperformed other approaches (p < 0.05 Wilcoxon sign-rank test) with a median DSC of 0.93, a median MSD of 0.45 mm, and a median HD of 2.61 mm. For the left thalamus, no approach significantly outperformed the others. Finally, for the right thalamus, no approach significantly outperformed the others.

4. Discussion

In this work, we presented segmentation approaches for segmenting six subcortical structures bilaterally. These segmentation approaches considered the effect of imaging modality on segmentation results. Two distinct imaging modalities were considered. First, a standard T1-weighted MPRAGE, a sequence commonly acquired in clinical and research settings, was acquired for nine subjects. Second, a T1-weighted FGATIR, a specialized sequence with enhanced contrast in subcortical structures, was acquired for the same nine subjects. A series of 7 T T1-weighted MPRAGE scans with varying inversion times and high-resolution susceptibility weighted slabs were acquired on the nine subjects. Then, an expert in subcortical anatomy manually delineated the thalamus, putamen, internal and external globus pallidus, sub-thalamic nucleus, and substantia nigra bilaterally.

These nine subjects were then used in a leave-one-out cross-validation to assess the segmentation accuracy using only T1-weighted MPRAGE, only T1-weighted FGATIR, and multi-modally with the MPRAGE and FGATIR. In general, the multi-modal segmentation outperformed the other approaches and furthermore including atlases flipped laterally tended to improve segmentation results, but there was no single approach that outperformed in all cases. Fortunately, the proposed segmentation approach does not require all segmentations to be performed with the same modalities. This allows flexibility in which sequences are used to segment each structure. From a practical perspective, the lack of a globally best method is disappointing as it would seem to necessitate that different methods would be needed for different structures. We choose to view this result in a more positive light in that pragmatic segmentations are possible with a variety of different imaging modalities. Hence, it is possible to consider tradeoffs in imaging time, sequence availability, and segmentation approaches when designing a study to use multi-modal MRI for segmentation of subcortical structures.

Several recent works have used multi-modal MRI to deal with subcortical structure segmentation. Traynor et al. showed that adding T1 with T2 MRI improve thalamus segmentation based on a priori anatomical hypothesis and T1/T2 values [18]. Hasan et al. utilized T1, T2 and DTI maps to identify lesions appearance frequency in cerebral subcortical, lobar white and cortical grey matter subdivisions [19]. Haegelen et al. evaluated the effectiveness of using T1 and T2 MRI on
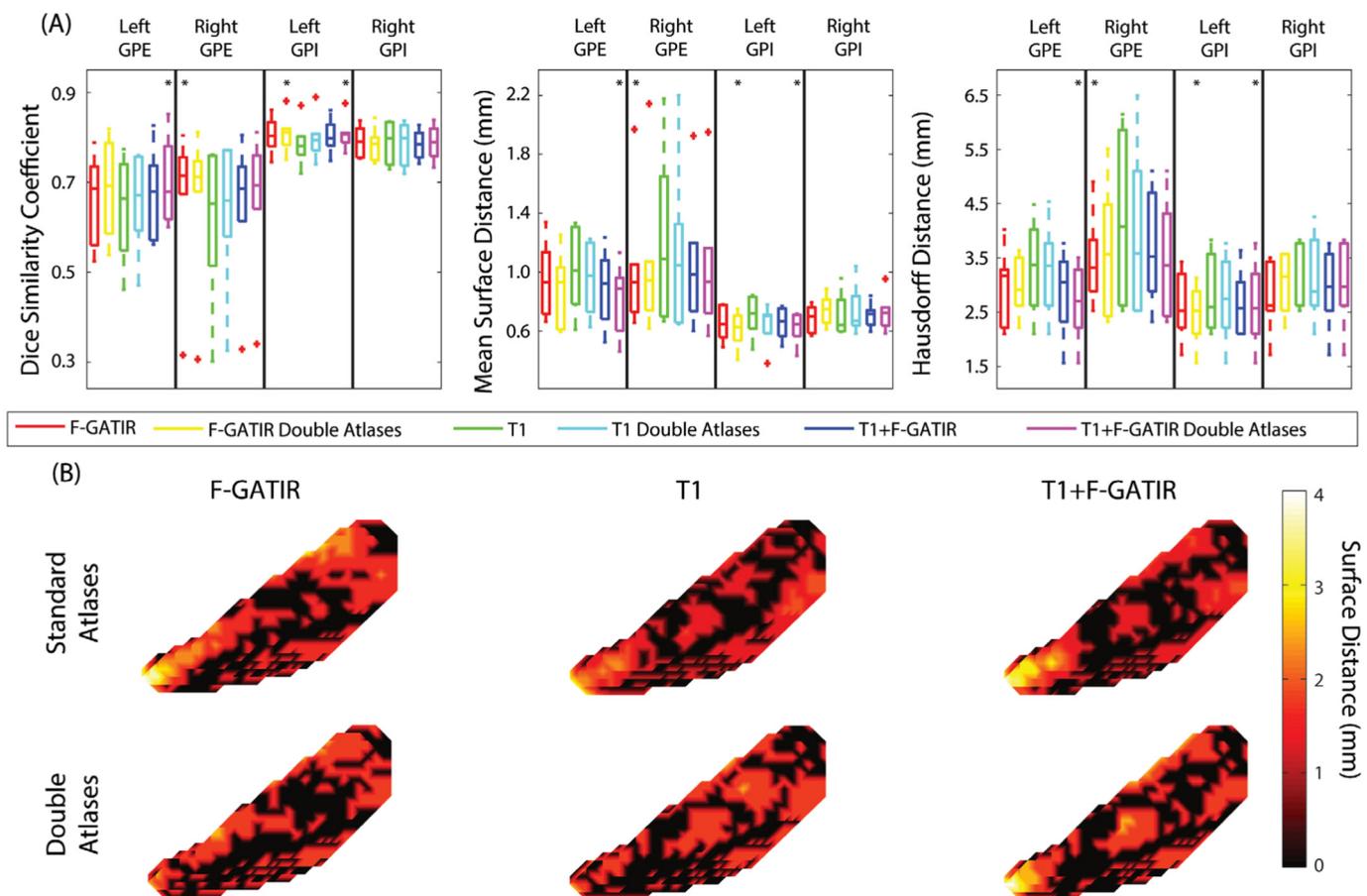
Fig. 2. Segmentation results for structures in the globus pallidus. Quantitative segmentation results are shown in (A). For the left GPE, multi-modal segmentation with T1 and FGATIR with double atlases outperformed other approaches (*; p < 0.05; Wilcoxon sign-rank test). For the right GPE segmentation with FGATIR outperformed other approaches (*; p < 0.05; Wilcoxon sign-rank test). For the left GPI, multi-modal segmentation with T1 and FGATIR with doubled atlases and segmentation with FGATIR with doubled atlases outperformed other approaches but were not distinguishable amongst each other (*; p < 0.05; Wilcoxon sign-rank test). For the right GPI no segmentation approach outperformed other approaches. In (B), surface distances between the true and estimated segmentations for the left GPI are shown for the six proposed segmentation approaches.

different registration approaches and the patch-based method to identify deep brain structures [20]. Similarly, Xiao et al. proposed patch based label fusion methods to segment the STN and its adjacent structures using T1 and T2 MRIs [21]. Forstmann et al. presented a data set that includes whole-brain and reduced field-of-view T1 MP2RAGE and T2-W scans of the subcortex and brainstem with an ultra-high resolution at a sub-millimeter scale, and the data can be used to develop new algorithms that help to build high-resolution atlases [22]. For instance, Visser et al. use Forstmann's dataset multimodal (T1, T2, and DTI) method for subcortical segmentation and apply it to the striatum and globus pallidus, substantia nigra, subthalamic nucleus and red nucleus [23,24]. D'Albis et al. developed PyDBS, which is an automated image processing workflow for deep brain stimulation surgery that integrates with a T1-T2 multi-modality input pipeline [25]. Liu et al. showed a multi-modal (T1 and T2) learning-based method using regression forests to automatically localize the target in pre-operative MR brain scans [26]. Ewert et al. used T1, T2, proton density, T2 relaxometry to parcellate STN and GPi functional zones using structural connectivity to the cortex and the thalamus respectively [27]. Kim et al. demonstrated that Susceptibility Weighted Image (SWI) and T2 approach significantly improves volumetric segmentation subcortical structures such as the basal ganglia and thalamus at 7 T [28]. Coron et al. employed T1-, T2-weighted and quantitative susceptibility mapping (QSM) information to automatically segment major thalamic subnuclear groups [29]. Li et al. proposed a QSM/T1 multi-atlas approach to segment subcortical on QSM images [30]. We note that the Dice accuracy is imperfect on the

smaller structure (e.g., ~0.6 for the substantia nigra and STN). For population studies, this may be sufficient to detect group differences. However, careful consideration of the spatial accuracy would be needed before interventional applications would be advised.

These sequences that we proposed in this work are of interest because they are all acquirable on a clinical population. As a result, the proposed segmentation approaches can be translated to clinical populations and thus aid in the clinical workflow. In particular, the STN and GPI are common targets for deep brain stimulation surgery (DBS) [31]. DBS is a surgery commonly used in Parkinson's disease to mitigate the motor symptoms of the disease. Generalization for pathological anatomies will require additional evaluation to ensure that the registration procedures can adapt between controls and patients. Alternatively, patient atlases could be acquired. Overall, this work is a meaningful step toward understanding the effects of imaging sequence on segmentation of subcortical grey matter structures and optimizing the algorithms for segmentation of these data.
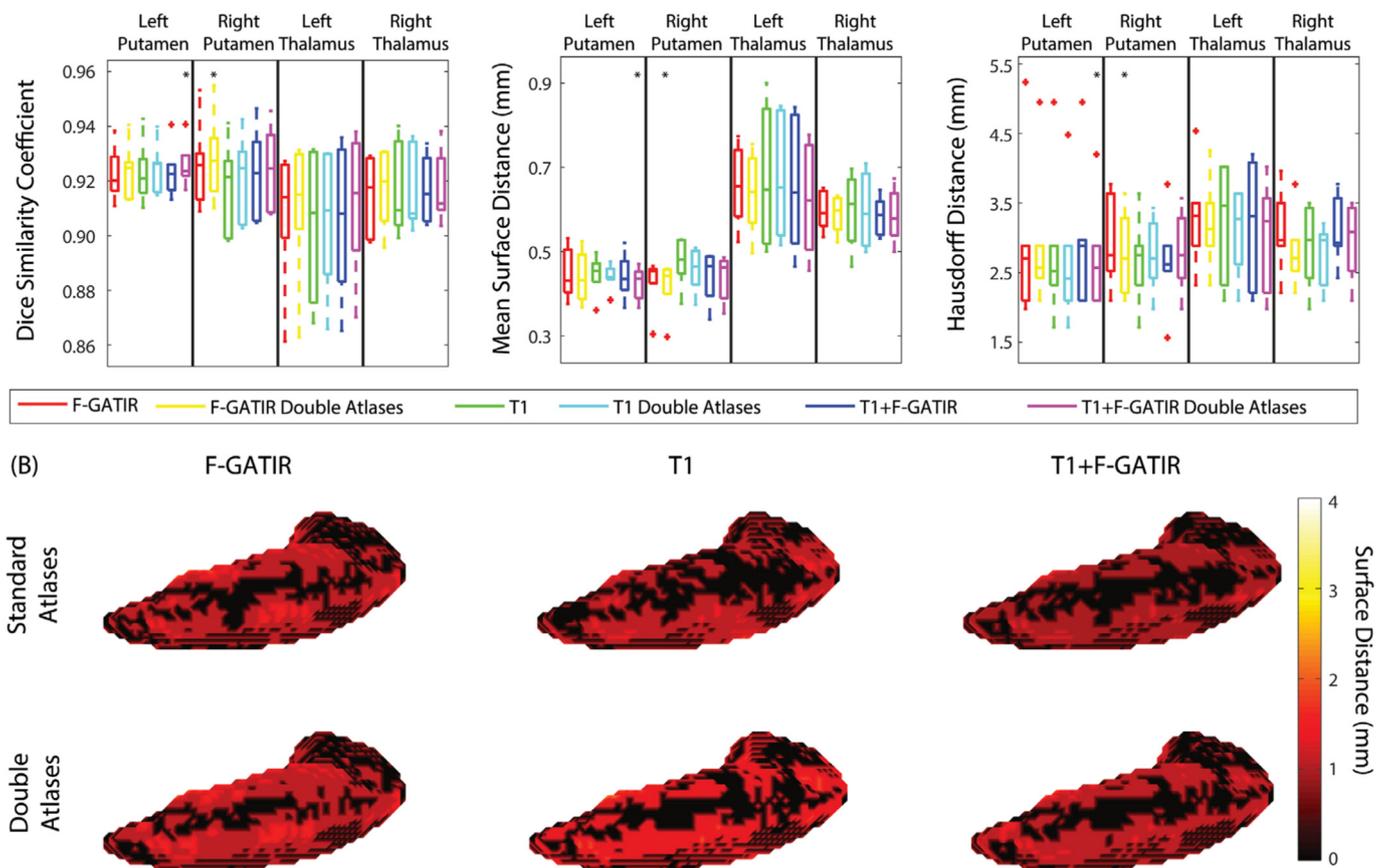
Acknowledgements

Fig. 3. Segmentation results for the putamen and thalamus. Quantitative segmentation results are shown in (A). For the left putamen, multi-modal segmentation with T1 and FGATIR with double atlases outperformed other approaches (*; $p < 0.05$; Wilcoxon sign-rank test). For the right putamen segmentation with FGATIR with doubled atlases outperformed other approaches (*; $p < 0.05$; Wilcoxon sign-rank test). For the left thalamus, no segmentation approach outperformed other approaches For the right thalamus, no segmentation approach outperformed other approaches. In (B), surface distances between the true and estimated segmentations for the left putamen are shown for the six proposed segmentation approaches.

References

[1] Alexander GE, Crutcher MD. Functional architecture of basal ganglia circuits: neural substrates of parallel processing. Trends Neurosci 1990;13(7):266–71.

[2] Albin RL, Young AB, Penney JB. The functional anatomy of basal ganglia disorders. Trends Neurosci 1989;12(10):366–75.

[3] Yin HH, Knowlton BJ. The role of the basal ganglia in habit formation. Nat Rev Neurosci 2006;7(6):464–76.

[4] Brown P. Oscillatory nature of human basal ganglia activity: relationship to the pathophysiology of Parkinson's disease. Mov Disord 2003;18(4):357–63.

[5] Sudhyadhom A, Haq IU, Foote KD, Okun MS, Bova FJ. A high resolution and high contrast MRI for differentiation of subcortical structures for DBS targeting: the Fast Gray Matter Acquisition T1 Inversion Recovery (FGATIR). Neuroimage 2009;47:T44–52.

[6] Xiao Y, Beriault S, Pike GB, Collins DL. Multicontrast multiecho FLASH MRI for targeting the subthalamic nucleus. Magn Reson Imaging 2012;30(5):627–40.

[7] Jovicich J, et al. MRI-derived measurements of human subcortical, ventricular and intracranial brain volumes: reliability effects of scan sessions, acquisition sequences, data analyses, scanner upgrade, scanner vendors and field strengths. Neuroimage 2009;46(1):177–92.

[8] Addington J, et al. North American prodrome longitudinal study (NAPLS 2): overview and recruitment. Schizophr Res 2012;142(1):77–82.

[9] D'Haese P-F, et al. CranialVault and its CRAVE tools: a clinical computer assistance system for deep brain stimulation (DBS) therapy. Med Image Anal 2012;16(3):744–53.

[10] Klein A, Dal Canton T, Ghosh SS, Landman B, Lee J, Worth A. Open labels: online feedback for a public resource of manually labeled brain images. 16th annual meeting for the organization of human brain mapping. 2010.

[11] Iglesias JE, Sabuncu MR. Multi-atlas segmentation of biomedical images: a survey (in eng). Med Image Anal 2015;24(1):205–19. Aug https://doi.org/10.1016/j.media.2015.06.012.

[12] Marcus DS, Wang TH, Parker J, Csernansky JG, Morris JC, Buckner RL. Open Access Series of Imaging Studies (OASIS): cross-sectional MRI data in young, middle aged, nondemented, and demented older adults. J Cogn Neurosci 2007;19(9):1498–507.

[13] Asman AJ, Huo Y, Plassard AJ, Landman BA. Multi-atlas learner fusion: an efficient segmentation approach for large-scale data. Med Image Anal 2015;26(1):82–91.

[14] Avants BB, Tustison NJ, Song G, Cook PA, Klein A, Gee JC. A reproducible evaluation of ANTs similarity metric performance in brain image registration (in eng). Neuroimage 2011;54(3):2033–44. Feb https://doi.org/10.1016/j.neuroimage.2010.09.025.

[15] Asman AJ, Landman BA. Hierarchical performance estimation in the statistical label fusion framework. Med Image Anal 2014;18(7):1070–81. Oct https://doi.org/10.1016/j.media.2014.06.005.

[16] Avants BB, Epstein CL, Grossman M, Gee JC. Symmetric diffeomorphic image registration with cross-correlation: evaluating automated labeling of elderly and neurodegenerative brain (in eng). Med Image Anal 2008;12(1):26–41. Research Support, NIH, Extramural. Feb https://doi.org/10.1016/j.media.2007.06.004.

[17] Wang H, Suh JW, Das SR, Pluta JB, Craige C, Yushkevich PA. Multi-atlas segmentation with joint label fusion. IEEE Trans. Pattern Anal. Mach. Intell. 2013;35(3):611–23.

[18] Traynor CR, Barker GJ, Crum WR, Williams SC, Richardson MP. Segmentation of the thalamus in MRI based on T1 and T2. Neuroimage 2011;56(3):939–50.

[19] Hasan KM, Walimuni IS, Abid H, Wolinsky JS, Narayana PA. Multi-modal quantitative MRI investigation of brain tissue neurodegeneration in multiple sclerosis. J Magn Reson Imaging 2012;35(6):1300–11.

[20] Haegelen C, et al. Automated segmentation of basal ganglia and deep brain structures in MRI of Parkinson's disease. Int J Comput Assist Radiol Surg 2013;8(1):99–110.

[21] Xiao Y, et al. Patch-based label fusion segmentation of brainstem structures with dual-contrast MRI for Parkinson's disease. Int J Comput Assist Radiol Surg 2015;10(7):1029–41.

[22] Forstmann BU, Keuken MC, Schafer A, Bazin P-L, Alkemade A, Turner R. Multimodal ultra-high resolution structural 7-Tesla MRI data repository. Sci. Data 2014;1:140050.

[23] Visser E, et al. Automatic segmentation of the striatum and globus pallidus using MIST: multimodal image segmentation tool. NeuroImage 2016;125:479–97.

[24] Visser E, Keuken MC, Forstmann BU, Jenkinson M. Automated segmentation of the substantia nigra, subthalamic nucleus and red nucleus in 7 T data at young and old age. NeuroImage 2016;139:324–36.

[25] D'Albis T, Haegelen C, Essert C, Fernández-Vidal S, Lalys F, Jannin P. PyDBS: an automated image processing workflow for deep brain stimulation surgery. Int J Comput Assist Radiol Surg 2015;10(2):117–28.

[26] Liu Y, Dawant BM. Multi-modal learning-based pre-operative targeting in deep brain stimulation procedures. 2016 IEEE-EMBS international conference on bio-medical and health informatics (BHI). IEEE; 2016. p. 17–20.

[27] Ewert S, et al. Toward defining deep brain stimulation targets in MNI space: a subcortical atlas based on multimodal MRI, histology and structural connectivity. Neuroimage 2018;170:271–82.

[28] Kim J, Lenglet C, Duchin Y, Sapiro G, Harel N. Semiautomatic segmentation of brain subcortical structures from high-field MRI. IEEE J Biomed Health Inform 2014;18(5):1678–95.

[29] Corona V, Lellmann J, Nestor P, Schoenlieb C-B, Acosta-Cabronero J. A multi-contrast MRI approach to thalamus segmentation. arXiv preprint arXiv:1807.10757. 2018.

[30] Li X, et al. Multi-atlas tool for automated segmentation of brain gray matter nuclei and quantification of their magnetic susceptibility. NeuroImage 2019;191:337–49.

[31] Kahn E, et al. Deep brain stimulation in early stage Parkinson's disease: operative experience from a prospective randomised clinical trial. J Neurol Neurosurg Psychiatry 2012;83(2):164–70.